Pyramid wavefront sensing using Laser Guide Star for 8m and ELT class telescopes

Esposito, S., Agapito, G., Giordano, C., Puglisi, A., Pinna, E., et al.

S. Esposito, G. Agapito, C. Giordano, A. Puglisi, E. Pinna, C. Blain, C. Bradley, "Pyramid wavefront sensing using Laser Guide Star for 8m and ELT class telescopes," Proc. SPIE 9909, Adaptive Optics Systems V, 99096B (27 July 2016); doi: 10.1117/12.2234423

SPIE.

Event: SPIE Astronomical Telescopes + Instrumentation, 2016, Edinburgh, United Kingdom

Pyramid wavefront sensing using Laser Guide Star for 8m and ELT class telescopes

S. Esposito[a], G. Agapito[a], C. Giordano[a], A. Puglisi[a], E. Pinna[a], C. Blain[b], C. Bradley[b]

[a]Osservatorio Astrofisico di Arcetri, Largo E. Fermi 5, Firenze, Italy;
[b]University of Victoria Adaptive Optics Laboratory, Department of Mechanical Engineering, PO Box 1700, Stn. CSC, Victoria, BC, V8W 2Y2, Canada

ABSTRACT

Keywords: Adaptive Optics, Pyramid Wavefront Sensor, Shack-Hartmann Wavefront Sensor, Laser Guide Star, Spot Elongation

Laser Guide Stars (LGS) are mandatory to ensure large sky coverage of astronomical Adaptive Optics (AO) systems developed for 8m telescopes and Extremely Large Telescopes (ELT). However, the finite distance of the LGS spot from the telescope makes LGS wavefront sensing not easily scalable from an 8m to an ELT. The use of a Shack-Hartmann (SH) sensor with a Field-of-View (FoV) of about 10-20 arcsec requires fast (1kHz) very large detectors (more than 1000x1000 pixel for M4 5600 actuator) currently unavailable. In the paper, we present numerical simulations to study the behavior of a Pyramid wavefront sensor (PWFS) working with laser generated reference star. As detailed below, such a sensor can be implemented with existing CCD220. Achieved results are encouraging for both 8m and ELT class telescopes. In the 8m case, we studied a 40x40 sub-aperture configuration controlling about 800 modes and we achieved the same behavior as a SH sensor. For the 40m telescope, we considered a PWFS with 80x80 sub-aperture and we computed noise propagation coefficients up to mode 3000, showing an overall noise propagation residual of 54nm with 600 photons per sub-aperture. The simulated PWFS requires a small CCD with 176x176 pixel. We also run an end-to-end simulation: a SR of 70% at H band was achieved with a correction of 2100 modes. These results provide a first evidence that the PWFS can be used in the LGS based AO systems currently in design phase for 8m or 40m telescopes.

1. INTRODUCTION

Extensive simulations, laboratory experimentations and on-sky testing have been done for Shack-Hartmann wavefront sensor (SHS) used with LGS. Many algorithms (Weighted Center of Gravity (WCoG) [1], Correlation [2], Match Filter [3]) have been developed to optimize the spot centroid estimation when spot elongation and inhomogeneity are encountered with SHS.

The potential of PWFS [4][5] for next generation instruments is emphasized by the AO community. While PWFS and SHS loose part of their advantage when working with an extended object, using a PWFS could be advantageous for the following reasons:

- PWFS requires less pixels than a SHS using the Center-of-Gravity (CoG) spot location estimation. This is particularly relevant for ELTs where lowering the requirement on the number of CCD pixels would be beneficial for the future generations of AO instruments. Indeed, a 60 by 60 sub-apertures system with 10 by 10 pixels per sub-aperture would require a 600 by 600 pixel CCD. The current CCDs imager typically used in WFS have 240 by 240 pixel, so reducing the necessary number of pixels could greatly relax future CCD technical specifications.
- The PWFS FoV is adjustable during the observation by simply changing the field stop size. Again, using a PWFS would allow the use of a large pyramid optics instead of a very large CCD.
- Using a PWFS could reduce the negative impact of the spot elongation effect. Indeed, for SHS and PWFS, the extended object size will reduce the sensitivity, but the PWFS will not introduce any spot truncation effects typically encountered with SHS.

Adaptive Optics Systems V, edited by Enrico Marchetti, Laird M. Close, Jean-Pierre Véran, Proc. of SPIE Vol. 9909, 99096B
 · doi: 10.1117/12.2234423

A deeper understanding and estimate of PWFS performance when used with a LGS is therefore required to evaluate the feasibility and improvement that such a wavefront sensor could bring to the next generation instruments of 10 and 30-meter class telescopes. Several studies have been performed over the last decade [6][7][8]. Building upon previous simulations focused on the PWFS sensitivity when used with a 2D extended LGS [8], this paper presents the result of numerical analysis based on a 3D reference source, for which the thickness of the sodium layer has been taken into consideration.

Section 2 presents the implementation of the extended object in the simulator, section 3 studies the sensitivity of PWFS when using an extended object, section 4 and 5 show the results obtained for the 8m and 40m class telescopes respectively.

2. SIMULATOR IMPLEMENTATION

The extended object has been implemented in our end-to-end simulator software PASSATA [9] for both SHS and PWFS. For the SHS, a single propagation is made and the object elongation is added by means of a convolution with 2D kernels on the detector plane. These 2D kernels are computed considering the launcher, the sodium profile and the WFS geometry. Meanwhile, for the PWFS, the object is discretized in N points and for each point, p_i, a full PWFS propagation, up to the detector plane, is done. The final detector plane image, DP, is computed as a sum of the N detector plane images, DP_i, multiplied by the flux, f_i, of the single point (see Figure 1):

$$\mathrm{DP} = \sum_{\mathrm{i}=1}^{\mathrm{N}} \mathrm{f_i DP_i}\,. \tag{1}$$

As a result each point has the same input phase and different Tip, Tilt and Focus values. Note that N must be chosen to give good approximation of the extended object, and that the computing time is linearly proportional to N. The PWFS focal plane image, FP, is obtained as the sum of the N focal plane images, FP_I:

$$FP = \sum_{i=1}^{N} f_i FP_i\,. \tag{2}$$

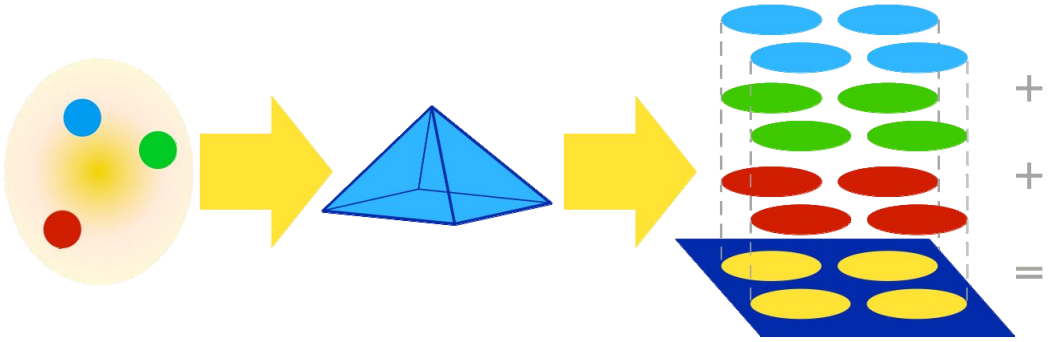

Figure 1. Scheme of the extended object implementation

3. 8M-CLASS TELESCOPES SENSITIVITY ANALYSIS

To estimate the sensitivity $\varsigma_{e(i,j)}$ of the PWFS when using a LGS, a positive KL mode is applied and the PWFS signals, S_x and S_y, are measured for each point of the extended object. These signals are obtained by computing the difference between the 4 quadrants (see Figure 1) as shown in Equation (3).

$$S_x = \frac{I_2+I_4-I_3-I_1}{\sum_{i=1:4} I_i} \;;\; S_y = \frac{I_1+I_2-I_3-I_4}{\sum_{i=1:4} I_i} \tag{3}$$

The same measurement is reproduced with the equivalent but negative KL mode and for each point, the RMS of the difference between the positive and negative signals obtained are recorded. These values are then displayed as a 2D maps for each layer (see Figure 2 left). The sensitivity estimation is repeated for mode 3, 50, 100 and 600 and for different PWFS modulation amplitude.

Figure 2 shows the sensitivity analysis for the KL mode 3 for different modulation amplitudes (0 to 10 λ/D).

In order to determine if the pyramid sensitivity can be improved by a given modulation amplitude, the sensitivity $\varsigma_{e(i,j)}$ of each point of the extended object was summed and a global sensitivity ς_g was estimated following equation (5) where $F_{(i,j)}$ is the flux for a given point of the extended object.

$$\varsigma_g = \sum_{i,j} \varsigma_{e(i,j)} * F_{(i,j)} \quad (5)$$

The resulting plot, presented in Figure 2 (right), confirms that modulating the pyramid does not provide an improvement for its overall sensitivity. This figure shows also that when the mode's order increases, the sensitivity of the PWFS grows because the points located far from the apex and edges start to rise.

Adding modulation increases the computational weight in the simulations. As a result, the closed-loop (CL) simulations made in this work have been performed without modulating the pyramid.

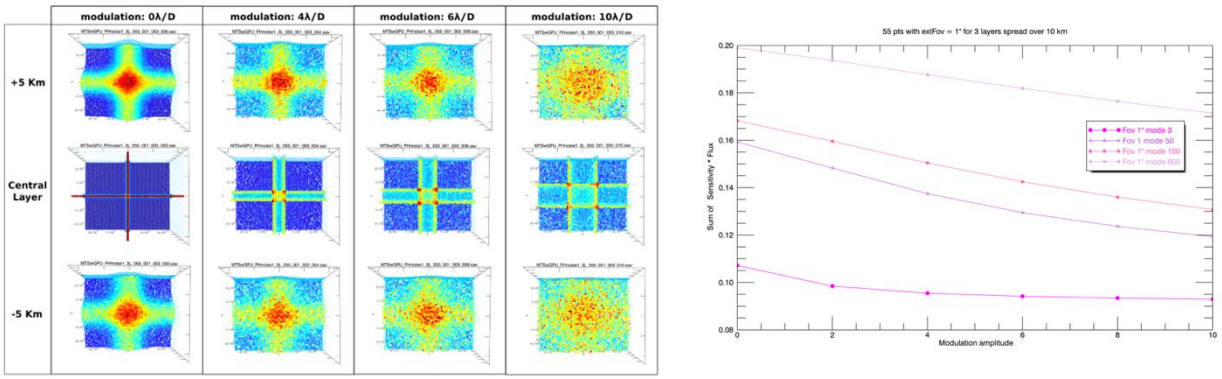

Figure 2. Left: sensitivity map obtained for mode 3 with modulation amplitudes of 0λ/D, 4λ/D, 6λ/D and 10λ/D. Right: global RMS sensitivity ς_g versus modulation amplitude for modes 3, 50, 100 and 600.

4. 8M SIMULATIONS

This section deals about the simulation of the PWFS working with extended sources, created by a LGS, on an 8m telescope. The instrument and atmosphere parameters used for the simulations are taken from the VLT conditions and are summarized in Table 1.

Table 1. Parameters of the telescopes and the atmosphere used for the simulations

Parameter			Value
Telescope	Entrance Pupil Diameter	D	8.118 m
	Central Obscuration ratio	ε	15.9 %
Atmospheric conditions	Seeing	ε_0	0.87 arcsec (@500nm)
	Outer scale	L_0	22m
	No. Layers		10 [10]
LGS detected flux			100ph/sub-ap./ms
Deformable mirror			1170 Influence Functions from FEA model of the DSM

Parameter			Value
	Conjugated height		0m
LGS WFS	Type		Pyramid
	No. sub-aperture		40x40
	FoV		2.35 arcsec diameter (PWFS) 5.0 arcsec diameter (SHS with 6x6 pixels/sub-ap.)
	Central Wavelength	λ_{wfs}	589nm
AO RTC	Max frame frequency		1 kHz
	Control		Modal control with static modal gains
	Reconstruction matrix		Pseudo-inverse
	Temporal controller		Simple integrator
	Total time delay		3ms
LGS specific information	LGS spot FWHM		0.8 on-sky arcsec
	Laser launcher position		Centered on the mirror
	Sodium layer		"Single Peak" sodium profile (from [11] with UTC = 20080717 – 06_40_56) with a sampling of 1km (16 layers)
	Focus Height		92.4km

4.1 Calibration

As one can see in Table 2, the computational time for a sampling of 1λ/D is rather big and does not allow us to explore a large range of configurations for making end-to-end simulations. As a result, we decided to check that an in-plane discretization of the extended object, with a sampling of 4λ/D, gives almost equivalent results than a denser sampling. Figure 3 (left) shows the Noise Propagation Coefficients (NPC) and these results allow us to choose this sampling and to reduce the computation time of a factor 16.

Then we compared the NPCs of:

1. a PWFS with circular modulation of ±19λ/D.
2. a PWFS with a 2D extended object with a Gaussian intensity map (FWHM = 0.8").
3. a PWFS with a 3D extended object with an in-plane Gaussian intensity map (FWHM = 0.8") and the vertical intensity profile shown in [11] with UTC = 20080717 – 06_40_56.
4. a SH with the same 3D extended object than for the aforementioned PWFS.

Figure 3 (right) shows that all these NPCs are very close to each other. The ones obtained for the modulated PWFS and the 2D extended object are similar because the value of the radius of modulation corresponds to the mean radius of the Gaussian with a Full-Width-Half-Max (FWHM) of 0.8". Moreover, the PWFS with 2D and 3D extended object show similar sensitivity because the vertical extension has a minor impact w.r.t. the in-plane extension. Indeed, the RMS of the tip corresponding to an angle of 0.4" (equal to the FWHM/2) is about 4 times the one of a defocus, corresponding to a distance of 3.5km (the sodium profile FWHM is ~7km). Finally, the SH and the modulated PWFS have the same sensitivity because the modulation diameter is almost equal to λ/d where d is the sub-aperture size [12].

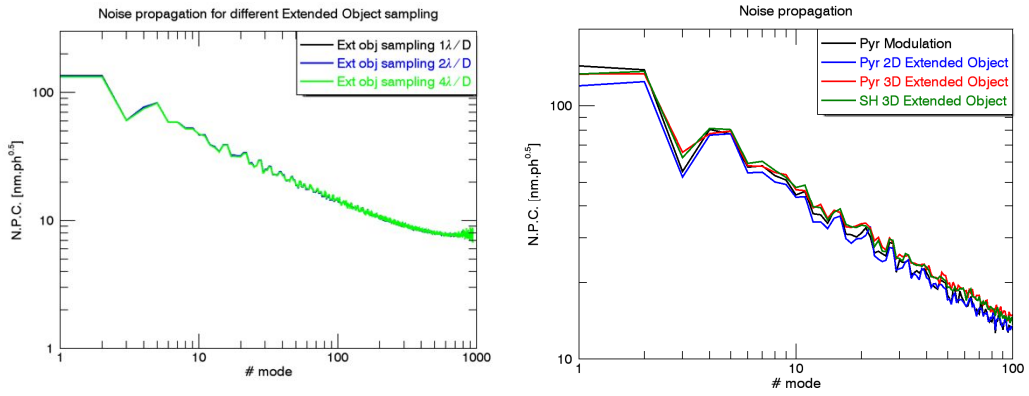

Figure 3. Left: NPC for a PWFS with a 2D extended object and different spatial sampling. Right: NPC for ±19λ/D modulation (black line), 2D extended object (blue line), 3D extended object (green line) and SH with 3D extended object (red line).

Table 2. Simulation times for different extended object horizontal sampling.

Sampling [λ/D]	1	2	4
# points / layer	7936	1992	492
# points total	126976	31872	7872
time/step [s]	23.5	5.9	1.5

4.2 End-to-end simulations

After the sensitivity analysis, we ran Single Conjugated AO (SCAO) and Multi Conjugated AO (MCAO) simulations. The SCAO parameters are shown in Table 1. The results are summarized in Table 3 and Figure 4. The performances of the two WFSs are comparable with small differences in Strehl Ration (SR) and in the modal residuals. Note that we do not take into account the conical error and we use a cylindrical propagation.

As second configuration, we choose a MCAO system as described in [13]. From this paper, we can notice that the performances of the two WFSs are almost equivalent.

Table 3. SCAO performances using only cylindrical propagation.

WFS	**SR H band**	
	without noise	with photon noise
SH	88.5	86.4
Pyramid	89.8	87.1

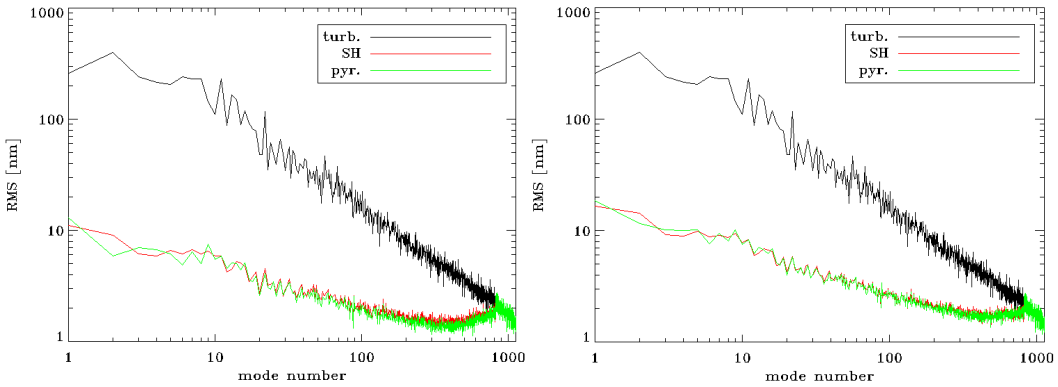

Figure 4. Turbulence and residual modal plots obtained for a LGS SCAO with cylindrical propagation. Left: without noise, right: with photon noise. Comparison between Pyramid (green) and SH (red) WFS. 40x40 sub-aperture, 819 modes corrected, 3 frames of delay, int. gain 0.5. Pyramid WFS has FoV=2.35" and 4λ/D sampling. SH WFS has FoV=5.0" with 6x6 pixel per sub-aperture.

5. GOING FROM 8M TO 40M-CLASS TELESCOPES

Up to now, the computation time has not been a major issue as shown in Section 4, but for the 40m-class telescopes, it can be a showstopper. In fact, the computation time to simulate the PWFS with an extended object greatly increases as the telescope diameter size scales from 8 to 40m. Below, we list all the issues related to the telescope diameter increase.

- Horizontal extension of the object: a factor 5 in diameter (compared to the 8m-class telescopes) means that the λ/D sampling on the sodium layers is 5 times lower, and as a result, the number of points increases by a factor 25. Even the phase array, to maintain the same sampling, increases 5 times. Thus, we will have to do 25 times more FFTs of arrays 5 times bigger.
- Vertical extension of the object:
    - As can be simply demonstrated using the thin lens equation, the FoV requested by the WFS, to sense properly the out of focus layers, is linearly proportional to the diameter. So the FoV must be 5 times the one of the 8m-class telescope. Moreover, we must increase the phase sampling by the same factor 5 to increase the WFS FoV.
    - The focus coefficient given by the out of focus layers depends on the square of the focus length, and so on the square of the diameter. For the 8m-class telescope, we choose a vertical sampling of 1km, which corresponds to a step of approximately 3 radians RMS of Zernike focus. The same step of Zernike focus for a 40m-class telescope is given by a 40m vertical sampling. Hence, the vertical sampling increases also by a factor 25.

Combining all these issues, we can conclude that we have to do 625 more FFTs of arrays that are 25 times bigger. As a result, the time of a simulation step will be about ~25000 time the one of an 8m class telescope (FFT computation time scale as $n\log(n)$). It is clear that we have to find methods to reduce such time so that we can run calibrations and simulations in few days.

Hence, we decided to make the following approximations:

- Use a D.L. modulation instead of a discretized Gaussian object. As is shown in Figure 3 and in [7][14] a D.L. modulation with an equivalent radius (r=FWHM/2.95) gives NPC very similar to the one given by a discretized Gaussian shaped object. This reduces the number of FFTs by a factor ~150 for a λ/D sampling equal to 1.
- Use a combination of two samplings for the sodium vertical profile. We choose a sampling of 100m in the range ±500m from the in-focus layer and 1km outside this range. This gives a factor ~15 on the number of FFTs. Figure 5 (left) shows that the NPC with this sampling is very similar to the one obtained with the 40m sampling. This sampling is chosen because the WFS signal changes more near the in-focus layer and less far from it (see center part of Figure 5). In fact, far from the in-focus layer, the majority of the WFS slopes have a value of zero because they are saturated by the focus (see right side of Figure 5).

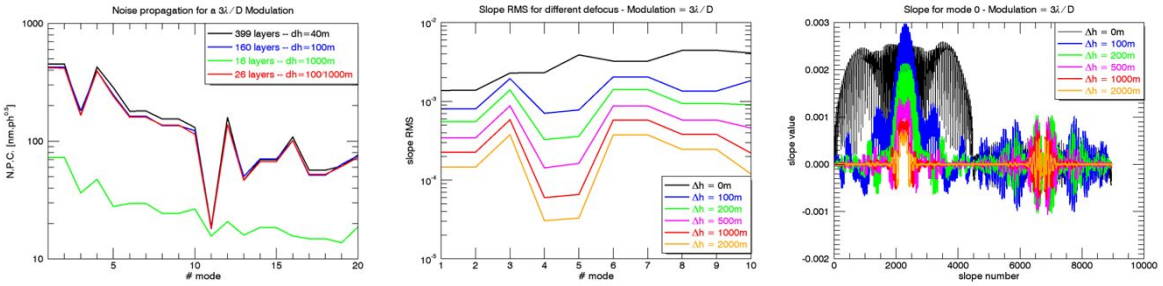

Figure 5. Effects of sodium profile for a modulated D.L. object (modulation ±3λ/D). Left: Noise Propagation Coefficients (NPC) for different vertical sodium profile samplings. Center: Slope RMS. Right: Tip slope 1D representation with out-of-focus distances from 0m to 2000m.

5.1 Noise propagation coefficients and error budget

With the changes described in the previous section, we computed the NPCs for the PWFS and the SHS. These coefficients, presented in Figure 6, show that:

- The difference between the 2D and 3D extended object is larger than the one for the 8m case (Figure 3). Indeed, for the 40m-class telescope, the vertical extension has a greater impact than the in-plane extension. The RMS of the tip, corresponding to an angle of 0.4" (equal to the FWHM/2), is about 75% the one of a defocus corresponding to a distance of 3.5km (sodium profile FWHM is ~7km).
- The PWFS does not have a better sensitivity than the SHS because the size of the LGS object reimaged on the PWFS focal plane is equal, on average, to the SH lenslet spot size.

Thanks to these coefficients and analytical expressions for fitting and temporal errors [15] we can compute the AO system error budget. In fact, the estimation of photon noise error propagated through the reconstruction matrix can be extracted from the NPCs. This error is given by the following equation:

$$\sigma^2_{noise} = \kappa \sum_{i \geq 6} \frac{c_i^2}{f}, \tag{6}$$

where κ depends on the gain and the total loop delay (κ=0.8 for a gain of 0.5 and a delay of 2 frames), c_i is the value of the NPC for the ith mode and f is the flux assumed 600 ph./sub-ap./ms, consistent with LGS data [10][16]. The total AO residual error can be computed as (we neglect aliasing error):

$$\sigma^2_{tot} = \sigma^2_{fit} + \sigma^2_t + \sigma^2_{noise}\,. \tag{7}$$

The values are shown in Table 4: the total error for both WFS, with 2100 corrected modes, is about 165nm RMS corresponding to 67% SR in H band.

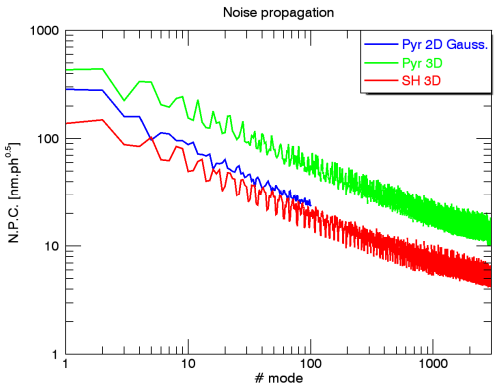

Figure 6. NPCs for 40m class telescope: PWFS with 2D extended object (blue line), and with 3D extended object (green line) and SHS with 3D extended object (red line).

Table 4. Expected errors for Pyramid and SH WFSs.

WFS	**No. of corrected modes**	**Expected errors [nm RMS]**			
		Fitting	Photon noise	Temporal	Total
PWFS	2100	160	52	20	169
	3000	138	54	20	150
SHS	2100	160	18	20	162
	3000	138	19	20	141

5.2 40m-class telescope simulations

Finally, we ran a closed loop using PWFS and SHS. The parameters that differ from the ones for the 8m-class telescope simulations are summarized in Table 5.

For this pupil diameter, we run closed loops of a total time of 1s (integration time = 1ms) because the time needed for each iteration of the PWFS is very long (~10min). The turbulence and residual modal plot is shown in Figure 7 and the Strehl ratio obtained is 70% for both WFSs. These values are in good agreement with the ones found in Section 5.1.

It is worth noticing that in the simulations we considered only photon noise, but in real systems, the read-out noise will have a greater impact on SHS than PWFS because of the large number of pixels per sub-aperture.

Table 5. Parameters used for the 40m-class telescope simulations.

Parameters			**Values**
Telescope	Entrance Pupil Diameter	D	39 m
	Central Obscuration ratio	ε	0.283 %
Atmospheric conditions	Seeing	ε_0	0.67 arcsec (@500nm)
	Outer scale	L_0	25m
LGS detected flux			600ph/sub-ap./ms
Deformable mirror			4094 KL modes fitted on the E-ELT pupil
LGS WFS	No. sub-aperture		80x80
	FoV		8 arcsec diameter (PWFS) 10 arcsec diameter (SHS - with 20x20 pixels/sub-ap.)
	Central Wavelength	λ_{wfs}	589nm
AO RTC	Total time delay		2ms

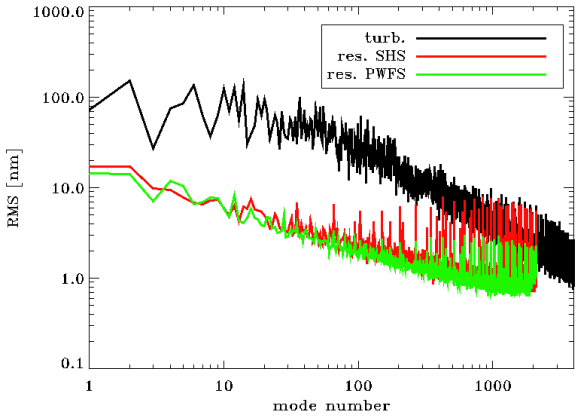

Figure 7. Turbulence and residual modal plot obtained for a LGS SCAO with cylindrical propagation and photon noise. Comparison between Pyramid (green) and SH (red) WFS with photon noise. 80x80 sub-aperture, 2100 modes corrected, 2 frames of delay, int. gain 0.5. Pyramid WFS has FoV=8.0". SH WFS has FoV=10.0" with 20x20 pixel per sub-aperture.

6. CONCLUSION

We studied with numerical simulations the behavior of PWFS with sodium LGS reference beacons for 8m and E-ELT class telescopes and compare it with a SHS. Our simulations take into account fully the 3D reference object created in the sodium layer. In the 8m case, we studied a 40x40 sub-aperture configuration controlling about 800 modes and we achieved the same behavior as a SH sensor. In the E-ELT case, we considered WFSs with 80x80 sub-aperture, a PWFS with a CCD patch of 176x176 pixel against a SHS with 1600x1600 pixels. We computed noise propagation coefficients up to mode 3000, showing an overall photon noise propagation residual of 54nm and 19nm respectively for PWFS and SHS using 600 phot/sub-ap./ms. Closed loop E2E simulations demonstrated a 70% SR in H band correcting 2100 modes for both WFSs. In other words, in the discussed case, the photon noise does not dominate the wavefront error budget. These results provide evidence that the PWFS can be used in the LGS based AO systems currently in design phase for 8m and/or 40m telescopes.

REFERENCES

[1] Nicolle, M., Fusco, T., Rousset, G., and Michau, V., "Improvement of shack-hartmann wave-front sensor measurement for extreme adaptive optics," Opt. Lett. 29, 2743–2745 (2004).
[2] Poyneer, L. A., "Scene-based shack-hartmann wave-front sensing: analysis and simulation," Appl. Opt. 42, 5807–5815 (2003).
[3] Gilles, L. and Ellerbroek, B. L., "Shack-hartmann wavefront sensing with elongated sodium laser beacons: centroiding versus matched filtering," Appl. Opt. 45, 6568–6576 (2006).
[4] Ragazzoni, R., "Pupil plane wavefront sensing with an oscillating prism", Journal of Modern Optics 43, 1-5 (1996).
[5] Esposito, S. and Riccardi, A., "Pyramid wavefront sensor behavior in partial correction adaptive optic systems," A&A 369, 9–12 (2001).
[6] Pinna, E., Puglisi, A. T., Argomedo, J., Quiros-Pacheco, F., Riccardi, A., and Esposito, S., "The pyramid wavefront sensor with extended reference source," in Second International Conference on Adaptive Optics for Extremely Large Telescopes, (2011).
[7] Quiros-Pacheco, F., Pinna, E., Puglisi, A., Busoni, L., Agapito, G., Rabien, S., and Esposito, S., "Pyramid wavefront sensor performance with laser guide stars", Third International Conference on Adaptive Optics for Extremely Large Telescopes (2013).
[8] Blain C., Esposito, S., Pinna E., Puglisi, A., and Agapito, G., "Use of Laser Guide Star with Pyramid Wavefront Sensor", Fourth International Conference on Adaptive Optics for Extremely Large Telescopes (2016).
[9] Agapito, G., Puglisi, A. and Esposito, S., "PASSATA: object oriented numerical simulation software for adaptive optics," Proc. SPIE 9909, in these proceedings (2016).

[10] Riccardi, A., et al. “The ERIS adaptive optics system”, Proc. SPIE 9909, in these proceedings (2016).
[11] Pfrommer, T. and Hickson, P., “High resolution mesospheric sodium properties for adaptive optics applications,” A&A 565, A102 (2014).
[12] Verinaud, C., “On the nature of the measurements provided by a pyramid wave-front sensor”, Optics Communications 233, 27-38 (2004).
[13] Esposito S. et al., “AOF upgrade for VLT UT4: an 8m class HST from ground,” Proc. SPIE 9909, in these proceedings (2016).
[14] Ragazzoni, R., Dioaliti, E., and Vernet, E., “A pyramid wavefront sensor with no dynamic modulation”, Optics Communications, 208, pp. 51 (2002).
[15] Beckers, J.M., “Adaptive Optics for Astronomy: Principles, Performance, and Applications”, Annual Review of Astronomy and Astrophysics 31, 13-62 (1993).
[16] Hackenberg, W., Bonaccini Calia, D., Lewis, S., Holzlohner, R., et al., “The Four-Laser Guide Star Facility (4LGSF) for the ESO VLT Adaptive Optics Facility (AOF),” Second International Conference on Adaptive Optics for Extremely Large Telescopes (2011).